

# Emulsion Templated Scaffolds that Include Gelatin and Glycosaminoglycans

Andrea Barbetta,<sup>\*,†</sup> Mara Massimi,<sup>\*,‡</sup> Biancalucia Di Rosario,<sup>†</sup> Stefania Nardocchia,<sup>†</sup> Marianna De Colli,<sup>‡</sup> Laura Conti Devirgiliis,<sup>‡</sup> and Mariella Dentini<sup>†</sup>

*Department of Chemistry, University of Rome “La Sapienza”, P.le A. Moro, 5, 00185 Rome, Italy, and Department of Basic and Applied Biology, University of L’Aquila, Via Vetoio, 67010 L’Aquila, Italy*

Received May 30, 2008; Revised Manuscript Received July 23, 2008

Gelatin is one of the most commonly used biopolymer for creating cellular scaffolds due to its innocuous nature. To create stable gelatin scaffolds at physiological temperature (37 °C), chemical cross-linking is a necessary step. In a previous paper (*Biomacromolecules* 2006, 7, 3059–3068), cross-linking was carried out by either radical polymerization of the methacrylated derivative of gelatin (GMA) or through the formation of isopeptide bonds catalyzed by transglutaminase. The method of scaffold production was based on emulsion templating in which an organic phase is dispersed in the form of discrete droplets into a continuous aqueous solution of the biopolymer. Both kinds of scaffolds were tested as culture medium for hepatocytes. It turned out that the enzymatic cross-linked scaffold performed superiorly in this respect, even though it was mechanically less stable than the GMA scaffold. In the present paper, in an attempt to improve the biocompatibility of the GMA-based scaffold, biopolymers present in the extracellular matrix (ECM) were included in scaffold formulation, namely, chondroitin sulfate and hyaluronic acid. These biopolymers were derivatized with methacrylic moieties to undergo radical polymerization together with GMA. The morphology of the scaffolds was tuned to some extent by varying the volume fraction of the internal phase and to a larger extent by inducing a controlled destabilization of the precursor emulsion through the use of additives. In this way, scaffolds with 44% of the void volume attributable to voids with a diameter exceeding 60 μm and with 79% of the interconnect area attributable to interconnects with a diameter exceeding 20 μm in diameter could be successfully synthesized. To test whether the inclusion of ECM components into scaffold formulation resolves in an improvement of their biocompatibility with respect to GMA scaffolds, hepatocytes were seeded on both kinds of scaffolds and cell viability and function assays were carried out and compared.

## Introduction

In spite of the great variety in the materials and methods employed in the fabrication of tissue engineering scaffolds, the principle of the scaffold designing remains clear: the scaffold should be designed by mimicking the native extracellular matrix (ECM) as much as possible, both in term of chemical composition and physical structure. Constructing a matrix or scaffold that simulates the ECM environment is therefore desirable and a widely used strategy in tissue engineering. Such a scaffold has the potential to promote cell growth and to restore key functions of damaged tissue and organs. The cells stimulated by appropriate scaffolds can remodel them and replace them with newly synthesized cell products.<sup>1</sup>

To mimic the high proportion of collagen present in most native tissue, collagen scaffolds are widely used in tissue engineering.<sup>2–5</sup> The prevalence of collagen in the majority of human tissue underlies its ability to support the growth of a wide variety of tissues, while its structure imparts favorable properties such as mechanical strength. However, collagen expresses antigenicity in physiological condition and, due to its scarce solubility, is difficult to process into a scaffold. The denatured-type collagen derived from the partial

hydrolysis of native collagen has been used in pharmaceutical and medical fields as sealants for vascular prostheses,<sup>6</sup> carriers for drug delivery,<sup>7</sup> wound dressings,<sup>8</sup> and tissue engineering.<sup>9–11</sup> It is well-known that gelatin also maintains many integrin-binding sites for cell adhesion and differentiation, which are found in collagen. Furthermore, gelatin is practically more convenient than collagen because a concentrated gelatin solution is soluble at temperature above 40 °C and is by far more economical than collagen. Previously, we have reported on a general method for scaffold synthesis based on high internal phase emulsion templating (HIPE) using various biopolymers<sup>12–14</sup> as the scaffold components. In particular, gelatin proved to be a versatile biopolymer in the preparation of scaffolds with the HIPE approach. Cross-linking among biopolymers chains was accomplished through a conventional radical polymerization of the vinylic functionalized gelatin chains or through the formation of isopeptide bonds between the γ-carbonyl group of a glutamine residue and the ε-amino group of a lysine residue catalyzed by microbial transglutaminase (MTGase). It was shown<sup>15</sup> through hepatocyte culture experiments that this latter cross-linking route preserved the biocompatible nature of the gelatin scaffolds better than the scaffolds obtained by radical polymerization. On the other hand, the latter type of scaffold possessed better mechanical properties. From the recognition that the biological function of human tissue is in large part due to the presence of other extracellular components such as glycosaminoglycans (GAGs), we wondered if the inclusion of naturally occurring GAGs within the methacrylated gelatin scaffold could improve sig-

\* To whom correspondence should be addressed. Tel.: +39 06 49913630 (A.B.); +39 0862 433290 (M.M.). Fax: +39 06 4457112 (A.B.); +39 0862 433273 (M.M.). E-mail: andrea.barbetta@uniroma1.it (A.B.); mara.massimi@univaq.it (M.M.).

† University of Rome “La Sapienza”.

‡ University of L’Aquila.

nificantly its performance in cell culture, while preserving or improving the mechanical properties of GMA scaffolds.

GAGs are negatively charged polysaccharides of different degrees of complexity, which are ubiquitous components of extracellular matrices and are, with the exception of hyaluronic acid, found in the form of proteoglycans on cell surfaces and in the extracellular space, where they exert various biological effects.<sup>16</sup> A number of GAGs, including chondroitin sulfate, dermatan sulfate, heparan sulfate, and hyaluronic acid, have also been found in liver tissue where they can actively influence hepatocyte proliferation and differentiation, directly or by interacting with other matrix components, such as fibronectin and laminin.<sup>17</sup>

In this study, chondroitin sulfate (CS) and hyaluronic acid (HA) were chosen as the model glycosaminoglycans and were bound to gelatin. Because of the good biological activities of gelatin, HA, and CS their combination may have beneficial effect on the biological characteristics of complex scaffolds.

In chondroitin sulfate, the disaccharide unit contains glucuronate and *N*-acetylgalactosamine and usually has one sulfate group per disaccharide, which is predominantly either in the 4 or 6 position on *N*-acetylgalactosamine. These highly charged units not only contribute to tissue hydration and elasticity but also may participate in the interaction with other extracellular matrix components.

Hyaluronic acid (HA), an abundant and virtually ubiquitous component of ECM, consists of 2-acetamido-2-deoxy- $\alpha$ -D-glucose and  $\beta$ -D-glucuronic acid residues linked by alternate (1–3) and (1–4) glycoside bonding. HA has a high capacity of water adsorption, water retention, and is believed to influence several cellular functions such as adhesion, migration, and proliferation.<sup>18,19</sup> As a consequence, HA plays a pivotal role in biological processes, including morphogenesis, tissue remodelling, differentiation, and injury healing. Recent biomedical applications of HA included scaffold for wound healing and tissue engineering,<sup>20–24</sup> as well as ophthalmic surgery, arthritis treatment, and as a component of implant materials. Attachment of GAGs may therefore offer the opportunity to exploit their biocharacteristics and valorise biomaterials like gelatin.

This paper is organized as follows: after the description of a method for HA degradation and the synthesis of the methacrylated derivatives of HA and CS, the preparation of scaffolds according to the HIPE methodology and the modulation of scaffold morphology are reported. Afterward, studies on the influence of scaffold composition (gelatin-methacrylate vs (gelatin-HA-CS)-methacrylate) on hepatocyte viability and function will be reported and discussed. Hepatocytes were chosen because they represent one of the models most widely used in biomaterial research.

## Materials and Methods

**Materials.** Gelatin A3 (G; extracted from porcine skin and with a Bloom number equal to 300) was supplied by Sigma-Aldrich. The surfactant Triton X-405 (70% w/v solution in water), methacrylic anhydride (MAA), 2,2'-azobisisobutyronitrile (AIBN), sodium chloride, dimethyl sulfoxide (DMSO), and toluene were purchased from Aldrich and used without further purification. Chondroitin 4- and 6-sulfate (CS) was purchased from Sigma Aldrich. Hyaluronic acid (HA) was a kind gift from Fidia Advanced Biopolymers (Abano Terme, Italy). Thermolysin (Protease X Bacillus thermoproteolyticus Rokko) and hyaluronidase (HYASE) extracted from calf testicles were purchased from Sigma.

**Degradation of HA.** The procedure described by Vercruyse et al. was followed.<sup>25</sup> HA (2 g) was dissolved in 400 mL of phosphate buffer

**Table 1.** Viscosimetric ( $M_\eta$ ), Numerical Weight ( $M_n$ ), Molecular Weights ( $M_w$ ), and Polydispersity ( $I$ ) of Hyaluronic Acid (HA), Degraded Hyaluronic Acid ( $HA_{deg}$ ), and Chondroitin Sulfate (CS)

samples	$M_\eta$ (Da)	$M_n$ (Da)	$M_w$ (Da)	$I$
HA	$1.5 \times 10^5$	$4.6 \times 10^5$	$9.8 \times 10^5$	2.11
$HA_{deg}$	$9.0 \times 10^3$	$1.0 \times 10^4$	$1.9 \times 10^4$	1.83
CS	$1.4 \times 10^3$	$3.5 \times 10^3$	$5.9 \times 10^3$	1.67

(pH = 6.4) and NaCl (16 mM) at room temperature. After complete dissolution, the temperature was raised to 37 °C and 57.34 mg of HYASE dissolved in 37 mL of phosphate buffer were added. A total of 45 min later, the solution was brought to boiling temperature to cause HYASE denaturation. After cooling and filtering through Millipore 3.0  $\mu$ m filters, the solution was put in dialysis tubes (molecular weight cut-off 1000) and dialysed against water. Finally the solution was freeze-dried. The degraded HA was then subjected to GPC analysis. The GPC used is a modular system (Laboratory flow 4000) with a refractometer (Shimadzu RID-10A). The samples were run using two TSK-GEL GM-PW (30 × 7.5, 17  $\mu$ m) columns and an aqueous solution of NaCl (0.01 N) as the mobile phase. The flow was set at 0.8 mL/min and the temperature at 25 °C. Calibration of the GPC was achieved using pullulan standards.

The kinetics of HA degradation was monitored by viscometry. Aliquots of HA were incubated at 37 °C with HYASE for prefixed times. At the end of each, the degradation was stopped by rising the temperature at 90 °C. Purification was carried out as described above. The intrinsic viscosity [ $\eta$ ] was determined using the viscosity measuring unit AVS379 (Schott-Gerate, Hofheim, Germany), connected to a Viscodoser AVS20 piston burette (for automatic dilutions), to make automated measurements of the flow-through times in a capillary viscometer (Ubbelholde viscometer,  $\Phi = 0.53$  mm, for dilution sequences). The viscometer was immersed in a precision water bath (transparent thermostat CT 1150, Schott Gerate, Hofheim, Germany) to maintain the temperature at 25 ± 0.1 °C. The solutions were prepared by dissolving the liophilized  $HA_{deg}$  with magnetic stirring for at least 24 h at room temperature, followed by filtration through a Millipore filter of 0.45  $\mu$ m. Solutions had relative viscosities from about 1.2 to 2.0 to ensure good accuracy and linearity of extrapolation to zero concentration. The intrinsic viscosity, [ $\eta$ ], was obtained by double extrapolation to zero concentration of Huggins' and Kraemer's equations, respectively

$$\frac{\eta_{sp}}{C} = [\eta] + k' [\eta]^2 C \quad (1)$$

$$\frac{(\ln \eta_{rel})}{C} = [\eta] + k'' [\eta]^2 C \quad (2)$$

where  $\eta_{rel}$  and  $\eta_{sp}$  are the (dimensionless) relative and specific viscosities,  $k'$  and  $k''$  are the Huggins' and Kraemer's coefficients, respectively, and  $C$  is the solution concentration.

**Preparation of Vinylated Derivatives.** Purification and functionalization of gelatin has been described in detail elsewhere.<sup>12</sup> Methacrylated hyaluronic acid (HAMA) was synthesised as follows: to a solution of 2% of  $HA_{deg}$  (see Table 1) in deionized water, NaOH (5 N, the mol ratio of MAA/NaOH is 1/1.12) was added. Then methacrylic anhydride (the mol ratio of MAA/HA-OH is 6/1) was added. The reaction solution was stirred at room temperature for 2 h and then moved into the refrigerator at 4 °C for 24 h. HAMA was dialysed (MW cut-off 1000) against deionized water until dialysis water reached the conductivity of distilled water and the final product was obtained by lyophilisation. A similar procedure was followed in the synthesis of chondroitin sulfate (CSMA) with the exception that in this case the mol ratio MAA/CS-OH was 18/1.

<sup>1</sup>H NMR (Bruker AVANCE AQS 600 MHz) operating at 600.13 MHz was used to determine the final functionality and purity of HAMA and CSMA ( $D_2O$ ).

**Preparation of Emulsion Templated Scaffolds.** The procedure for the production of (gelatin-hyaluronic acid-chondroitin sulfate)methacry-

late ((G-HA-CS)MA) based solid foams is as follows: the calculated amount of the vinylated biopolymers (total polymer concentration  $C_p = 20$  or 25% w/v, GMA/HAMA/CSMA = 80:10:10, wt/wt) was dissolved in 2.5 mL of water together with the surfactant Triton X-405 (net 7% w/v). This solution was placed in a three-necked round-bottom flask partially submerged in a water bath thermostatted at 50 °C to keep the solution containing gelatin in a liquid form. The flask was equipped with a dropping funnel consisting of a condenser connected to the thermostat and provided with a valve. This assured that the dispersed phase, 1% w/v of AIBN in toluene, was maintained at the same temperature of the biopolymer solution. The shear necessary for the dispersion of the organic phase into the continuous aqueous solution was provided by a D-shaped paddle driven by a mechanical stirrer set at 350 rpm. After completing the addition of toluene, the emulsion was kept under stirring for an additional 20 min, transferred into a cylindrical plastic container, and placed into an oven at 60 °C for one day. At the end of this time, the solid foam was soaked into DMSO, which was changed regularly (typically three times a day) for one week. This procedure was aimed to displace toluene thoroughly. The solid foam was then Soxhlet extracted with water for one day and finally freeze-dried.

**Characterization of (G-HA-CS)MA Scaffolds.** Foam morphologies were investigated with a LEO 1450VP scanning electron microscope (SEM). The inner area of fractured segments were mounted onto circular carbon adhesive pads attached to cylindrical aluminum stubs and were gold-coated using a sputter coater (SEM Coating Unit 953, Agar Scientific). Morphometry of void and interconnect diameters were conducted on micrographs obtained by light microscopy (Nikon 104 equipped with a JVC TK-1070 E video camera). Specimens were treated with a 5% w/v of glutaraldehyde in PBS buffer to strengthen their structure and were repeatedly washed with water to remove excess glutaraldehyde and then freeze-dried. Afterward, they were embedded with a resins (Lowcrys K4M, Polyscience). Sections, 1 μm thick, were cut with an ultramicrotome (UltracutE, Reichert Jung), collected on a glass slide, stained with a 0.1% w/v of an aqueous solution of Toluidine Blue and 0.1% w/v borax, and coverslipped by using Eukit balsam. The measurement of voids and interconnects (from a few to several hundreds, depending on polydispersity) was carried out on micrograph taken with the light microscope (LM) at a magnification of 200 and 400× using Scion Image (ScionCorporation) as a software tool. Raw data were used to calculate number-distributions of both voids and interconnects as well as their relative averages. These were then taken as the void and interconnect size of each porous matrix.

**Solid Foams Coding System.** All the solid foams synthesized are characterized by the same wt % ratio of GMA, HAMA, and CSMA. Thus, solid foams designation requires a simple code of the type:  $\phi X_{ab}$ , where  $\phi$  indicates the volume fraction of the dispersed phase defined as  $\phi = V_a/(V_a + V_o)$ , where  $V_a$  and  $V_o$  are the volumes of the aqueous and organic phases employed, respectively. When present,  $a$  and  $b$  indicate the presence and the concentration of additives either in the organic or the aqueous phase (DMSO and NaCl, 0.01 M). For instance, the code  $\phi 0.90_{D0.3,S}$  indicates a solid foam obtained from an emulsion characterized by a volume fraction of the dispersed phase of 0.9 and containing 0.3% v/v of DMSO with respect to the organic phase and NaCl (0.01 M) in the aqueous phase. Because in the cell culture experiments comparison between the matrices presented in this work and a gelatin methacrylate solid foam obtained in previous papers<sup>13,15</sup> is made, the latter will be designated GMA0.90<sub>D1,S</sub>. As before, 0.9 stands for the nominal fraction of the dispersed phase, while the suffix D1 and S indicate the presence of DMSO (1% v/v) and NaCl (0.01 M), respectively.

**In Vitro Biodegradation.** (G-HA-CS)MA or GMA (12.5 or 10 mg, respectively) solid foam was incubated in a thermolysin solution (5 μM in 0.05 M Tris-HCl, 2.5 mM CaCl<sub>2</sub>, 25 mg/L NaN<sub>3</sub>, pH = 7.4) thermostatted at 37 °C under mild stirring. Solution aliquots were placed into a quartz cell (thickness 0.5 cm) and analyzed with UV spectroscopy. The absorbance at 280 nm was monitored. The time for complete

dissolution of solid foam specimens was noted. The % of porous gel degradation is expressed as

$$\% \text{ degraded gel}(t) = A_{280}(t)/A_{280}(t_{\text{fin}})$$

where  $A_{280}(t)$  is the solution absorbance at time  $t$  and  $A_{280}(t_{\text{fin}})$  is the plateau absorbance corresponding to the completely dissolved gel.

**Culture of C3A Cells.** Human C3A/HepG2, purchased from the American type Culture Collection (ATCC, Manassas, VA), were suspended in RPMI 1640 medium (Sigma) supplemented with 10% (v/v) fetal calf serum (Gibco/BRL), 2 mM L-glutamine, 1% sodium pyruvate, 100 ug/mL streptomycin, and 100 U/mL penicillin (Sigma, St. Louis). Cells were seeded in 24-well culture plates containing UV-sterilized biomaterials and cultured at 37 °C in a humidified incubator in the presence of 5% CO<sub>2</sub>. The medium was changed 5 h after plating and, subsequently, every 2–3 days.

**Scanning Electron Microscopy.** The morphology of entrapped C3A cells was examined by SEM. After fixation in 2.5% glutaraldehyde in pH 7.5 phosphate buffer, cell-seeded scaffolds were dehydrated in a series of graded ethanol solutions (from 30 to 100%). Samples were then critical-point dried using liquid CO<sub>2</sub> and coated with 5 nm of vacuum-evaporated gold before examination on an XL 30 CP (Philips) SEM.

**Proliferation/Cytotoxicity Assays.** Cell adhesion and viability were determined 5 h after seeding and successively at time intervals of 2, 4, 8, 10, 15, and 18 days, by means of a MTS assay. Six small dishes (Ø 12 mm, approximately 140 mm<sup>3</sup> wet volume) were randomly cut from each cell-seeded scaffold and placed in 24-well plates; 20 μL of Cell Titer 96 AQ<sub>ueous</sub> One Reagent (Promega, Madison, WI) were then added into each well and left in contact with the cells for 3 h at 37 °C. MTS [3-(4,5-dimethylthiazol-2-yl)-5-(3-carboxymethoxyphenyl)-2-(4-sulphophenyl)-2H-tetrazolium] is bioreduced by metabolically active cells into a colored formazan product quantifiable by the absorbance at 490 nm. Values obtained in the absence of cells were considered as background. A standard curve was assessed to convert O.D. values to the number of viable cells, using cell densities ranging from 0 to 5 × 10<sup>5</sup> cells/well.

To determine the extent of cell damage, lactate dehydrogenase (LDH) release was quantified in supernatants using the LDH-cytotoxicity assay kit (BioVision, Mountain View, CA), as instructed by the manufacturer. For cell death estimation, cell membrane damage was expressed as percent of cell lysis.

**Live/Dead Cell Test.** C3A cells were stained with SITO 10, which stains viable cell green, and ethidium homodimer-2 (DEAD-Red), which stains cell nuclei red by entering into damaged cells, using the live/dead viability/cytotoxicity kit (Molecular Probes Inc., Eugene, OR). Stained cell-seeded scaffolds were observed under a confocal microscope (Sarastro 2000, Molecular Dynamics, Sunnyvale, CA) using an argon ion laser as a light source.

**Albumin Secretion Assay.** To assess hepatocyte metabolic activity, albumin secretion was monitored during the culture period (2, 4, 8, 10, 14, and 18 days) on both tridimensional (G-HA-CS)MA/GMA scaffolds and bidimensional polystyrene plates (IWAKY/polystyrene plates coated with gelatin (SIGMA), by an enzyme-linked immunosorbent assay (ELISA) using a human albumin kit (Bethyl Laboratories Inc., Montgomery, TX). Before the assay, wells were washed with PBS and fresh medium was added; after 24 h, this medium was withdrawn and aliquots were used for the specific albumin secretion assay. Human albumin was used to establish the standard curve. The levels of albumin were measured in different wells during the culture period and at each time point were normalized to the number of viable cells per well (ng/24 h/10<sup>6</sup> viable cells), as determined by the MTS assay. In parallel experiments, the time course of albumin secretion was assessed in long-term cultures by quantifying the albumin produced by cells from the same well throughout the culture period and reported in terms of ng of secreted protein/24 h. Each experiment was performed in triplicate.

**Statistical Analysis.** The student *t*-test was used to analyze the statistical significance of the data. Differences with a *p* value <0.05 were considered significant.

## Results and Discussion

**Degradation of HA.** An aspect of paramount importance when preparing a high internal phase emulsion (HIPE) is represented by the viscosity of the continuous phase. Experience<sup>26–32</sup> teaches that a too high viscosity of the continuous phase hinders the dispersion and homogenization of the internal phase. In the limiting case, only a relatively small quantity of the internal phase can be incorporated within the emulsion, thus preventing the formation of a HIPE (characterized, by definition, by a phase ratio  $\geq 0.74$ ). In such an event, the morphology of the ensuing porous materials is scarcely or not at all interconnected and characterized by a large polydispersity in void size.

As it is well-known, HA is a relatively stiff biopolymer as a consequence of its polyelectrolyte nature and network of intramolecular hydrogen bonding, the combination of which gives rise to a persistence length of 7–8 nm.<sup>33</sup> The viscous properties of HA in water is at the basis of its lubricating properties in the joints. In Table 1, the molecular weights of commercial HA and CS as well as their polydispersities are reported. While CS is characterized by a small molecular weight, HA has a  $\bar{M}_w$  close to  $10^3$  kD. We chose to use a % wt ratio among GMA, HAMA, and CSMA of 80:10:10 and a total polymer concentration in the aqueous phase of the emulsion of at least 20% w/v. The presence of GMA forced us to carry out HIPE formation at 50 °C, temperature at which GMA solutions are in fluid and, thus, in a processable state. Even at such a temperature the viscosity of the solution of the above specified blend of biopolymers was too high and prevented us from achieving a phase ratio of 0.74. It was evident that the cause of such a high viscosity was HA, because the successful preparation of GMA HIPE characterized by a  $\phi$  as high as 0.95 has been previously described.<sup>13</sup> As a consequence,  $\bar{M}_w$  of HA had to be reduced drastically. A simple, rapid, and regioselective way to achieve this goal is by enzymatic degradation. In mammals, three enzymes act in concert to degrade HA to its monosaccharide, that is, hyaluronidase,  $\beta$ -D-glucuronidase, and  $\beta$ -N-acetyl-D-hexosaminidase. Generally, the latter two enzymes cleave the oligosaccharides degraded by hyaluronidase (HYASE). It has been recognized that the reaction catalyzed by HYASE is the cleavage of internal  $\beta$ -N-acetyl-glucosamine at the reducing terminus and glucuronic acid at the nonreducing end.<sup>34</sup> Figure S1 (Supporting Information) shows the kinetics of HA degradation as monitored by the measurements of the changes in viscosity molecular weight ( $\bar{M}_v$ ). The steady viscosity molecular weight was reached within  $\sim 1$  h. Table 1 summarizes data relative to the molecular weights of HA, HA<sub>deg</sub>, and CS. In Figure S2 (Supporting Information), examples of the determination of the intrinsic viscosity through extrapolation of the Kramer and Huggins plots and GPC profiles for both HA and HA<sub>deg</sub> are shown.

Tests of emulsification using an aqueous solution of gelatin, HA<sub>deg</sub>, and CS (total polymer concentration = 20% w/v and a ratio of gelatin/HA/CS = 80:10:10 w/w/w) were successful. In the limiting case, a total polymer concentration of 30% w/v and a  $\phi = 0.95$  still gave a macroscopically homogeneous emulsion.

**Derivatization of HA and CS.** The synthesis of the methacrylated derivatives of HA and CS was carried out by employing well-established procedures.<sup>22,35</sup> Figure S3a,b (Supporting Information) shows the NMR spectra of CSMA and

HAMA, respectively. The degree of functionalization of HAMA (30%) was obtained by the ratio of the integrals of the signals relative to the vinyl protons (5.6–6.2 ppm) and of the proton in position 2 of the glucuronic residue of HA ( $\sim 3$  ppm). In the case of CSMA, the degree of derivatization (13%) was obtained by the ratio of the integrals of the peaks at 5.6–6.2 ppm, referring to the methyl protons of the methacrylate group at 2 ppm and the proton at position 2 of the glucuronic residue at 3.5 ppm.

**Synthesis of Emulsion Templated Scaffolds.** The preliminary, successful tests on emulsification by using HA<sub>deg</sub> induced us to explore the influence of  $\phi$  on scaffold morphology in the interval  $0.85 \leq \phi \leq 0.95$ . Total polymer concentration in the external phase ( $C_p$ ) was either 20 or 25% w/v for  $\phi \leq 0.90$  and  $\phi \geq 0.92$  solid foams, respectively. The increase of  $C_p$  was aimed at counteracting the weakness of the matrices resulting from the thinning of solid foam walls caused by the distribution of the continuous phase over an increasingly larger volume.

In Figure S4a (Supporting Information), an EDS spectrum puts into evidence the presence of sulfur belonging to the sulfate group of CS, and in Figure S4b (Supporting Information), the EDS sulfur map shows the homogeneous distribution of chondroitin sulfate within the scaffold walls. Figure 1 displays the SEM (column A) and LM (column B) micrographs of (G-HA-CS)MA solid foams arranged according to increasing  $\phi$ . Two features are clearly evident from a qualitative inspection of SEM micrographs: the considerable increase in void size for solid foams characterized by  $\phi \geq 0.90$  with respect to  $\phi 0.85$  and the thinning of solid foam walls. LM micrographs offer a clearer picture of the morphological changes consequent with the increase of  $\phi$ . In particular, the following feature is observable: the increase in void and interconnect size polydispersities. The void and interconnect diameter distributions were evaluated as a plot of their diameters obtained from LM micrographs as a function of the number of voids (interconnects) with the same size. Figure 2 shows the diameter distributions of the solid foams reported in Figure 1. In agreement with qualitative observations, both kinds of distributions become broader with the increase of  $\phi$ . LM micrographs allow a precise evaluation of the average void ( $\langle D \rangle$ ) and interconnect ( $\langle d \rangle$ ) diameters as well as their normalized polydispersities,  $\sigma_D/\langle D \rangle$  and  $\sigma_d/\langle d \rangle$ , respectively (Table 2).

The increase of both void and interconnect polydispersities are the results of mainly two factors: (1) the dependence of the emulsion viscosity on  $\phi$  and (2) the constancy of the surfactant concentration.

(1) Princen and Kiss,<sup>36</sup> Otsubo and Prud'homme,<sup>37</sup> and many others<sup>38–40</sup> have shown through experimental studies that the viscosity of HIPEs,  $\eta_{\text{HIPE}}$ , is proportional to  $\sigma$ ,  $\eta_e$ , and  $\phi$ , but inversely proportional to  $R$ , where  $\sigma$  is the interfacial tension,  $\eta_e$  is the viscosity of the external phase (dependent on  $\dot{\gamma}$ , the shear rate), and  $R$  is the droplet dimension. For a constant input of external energy (i.e., mechanical stirring) and viscosity of the external phase ( $C_p$  constant) as the volume of the added internal phase increases, the viscosity of the HIPE increases proportionally. This is also intuitive by considering that beyond the maximum packing of a homodisperse array of spherical droplets ( $\phi = 0.74$ ), the drops of the internal phase must take on a polyhedral shape to fit more tightly in the available space. Under shear, this array of droplets cannot slip past another like  $\phi \leq 0.74$  emulsions, but must first deform, and as a consequence, part of the supplied work will be dissipated. This is at the origin of the viscoelastic behavior of HIPEs and of the dependence of  $\eta_{\text{HIPE}}$  from  $\phi$ . Thus, during the process of

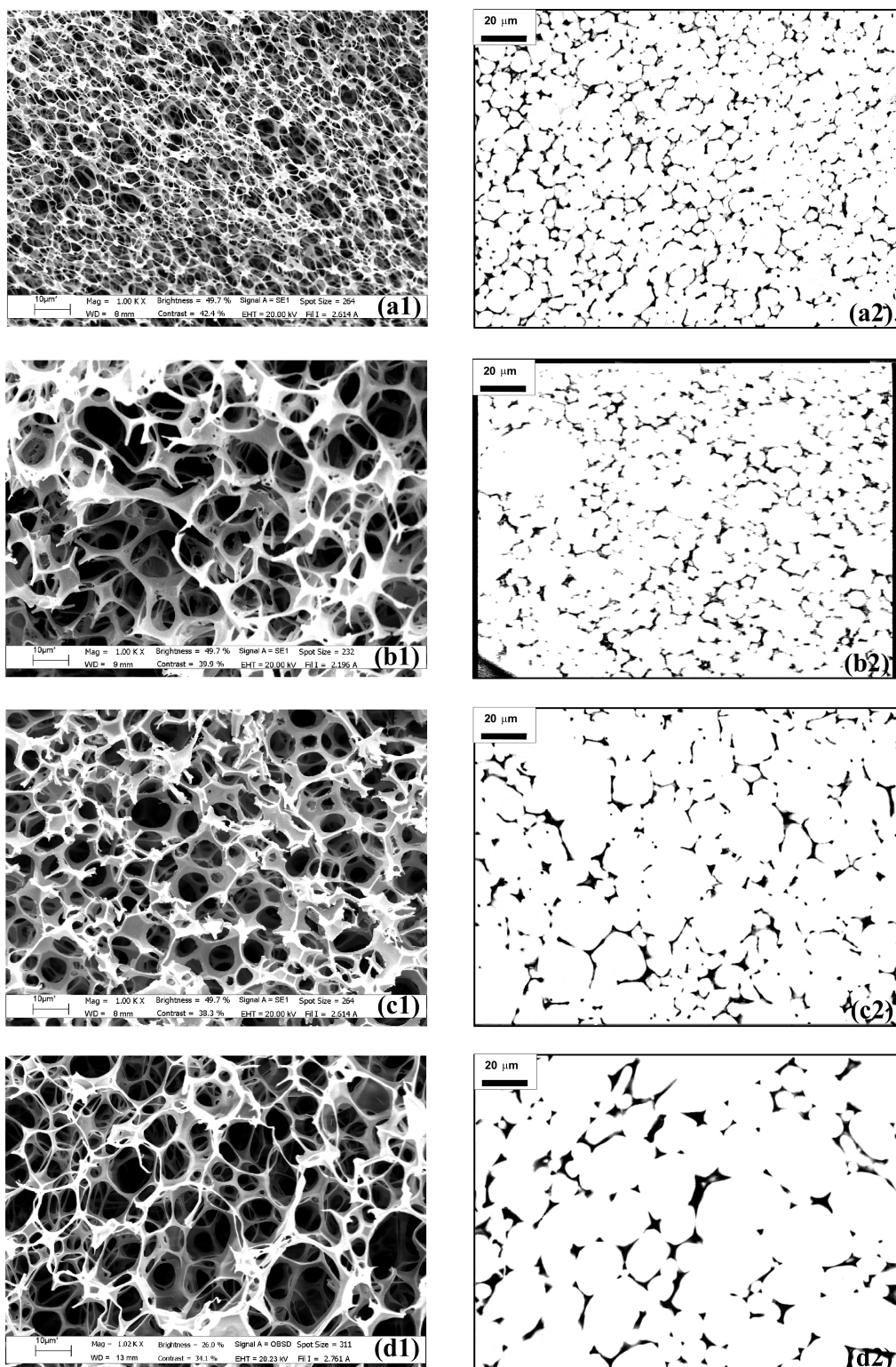


**Figure 1.** Scanning electron (1) and light (2) micrographs (magnification 400 $\times$ , scale bar 20  $\mu\text{m}$ ) of (G-HA-CS)MA polyHIPEs solid foams characterized by an increasing volume fraction of the dispersed phase ( $\phi$ ): (a) 0.85; (b) 0.90; (c) 0.92; (d) 0.95.  $C_p = 20\%$  w/v for the solid foams shown in (a) and (b), 25% w/v for the solid foams shown in (c) and (d), respectively.

addition of the dispersed phase as  $\phi$  increases, the constant shear stress supplied will encounter increasing difficulties in fragmenting the added dispersed phase into droplets and homogenizing into a collection of droplets characterized by narrow size distribution. As a result, high  $\phi$  porous structures tend to be characterized by a large polydispersity with respect to void size (Table 2).

(2) If the mass ratio of surfactant to continuous phase is constant, an increase in  $\phi$  gives a decrease in surfactant concentration (with respect to total HIPE volume), hence, an increase in interfacial tension,  $\sigma$ , and hence, an increase in void diameter ( $D$ ).

From Figure 2 it is evident that the whole distribution shifts toward the large diameter side as  $\phi$  increases and, at the same

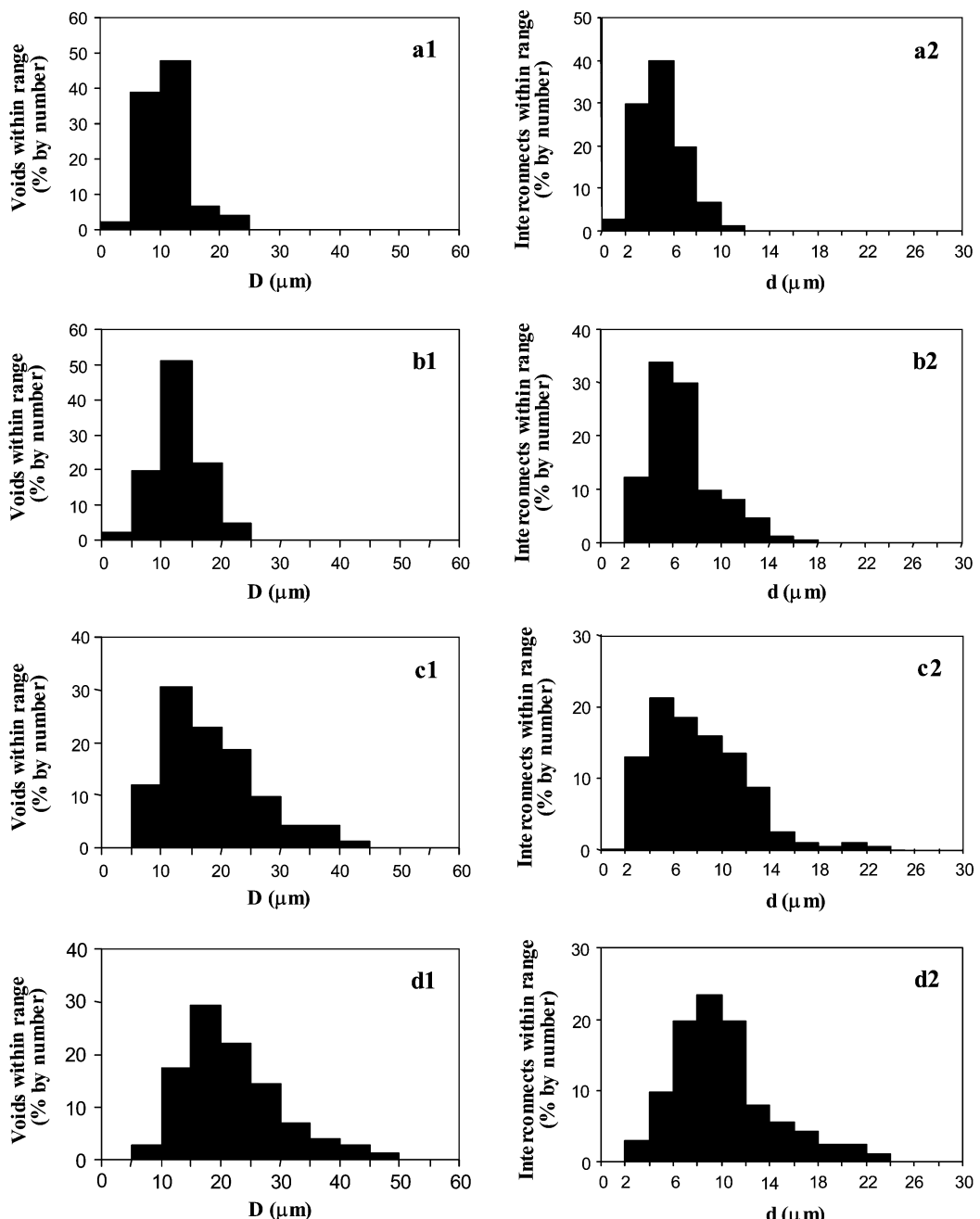


**Figure 2.** Number-distribution of voids (1) and interconnects (2) size of (G-HA-CS)MA solid foams characterized by an increasing volume fraction of the dispersed phase ( $\phi$ ): (a) 0.85; (b) 0.90; (c) 0.92; (d) 0.95. The area of a histogram is proportional to the number fraction of either voids or interconnects within a size range. Total polymer concentration: (a), (b) 20%; (c), (d) 25% w/v.

time, the contribution of voids in the diameter range 0–5 and 5–10  $\mu\text{m}$  decreases. A similar picture applies for interconnect diameter ( $d$ ). This behavior is the result of the two factors previously described operating at the same time. If the surfactant concentration in the water phase ( $C_s$ ) was scaled with the volume of the oil phase, only the viscosity of the emulsion would have influenced the droplet size population (and, as a result, the void size), and the proportion of small voids characterized by a  $D \leq 10 \mu\text{m}$  would have been left substantially unchanged. The position of the maximum of the void and interconnect distribution of the solid foams characterized by  $\phi \leq 0.92$  is independent from  $\phi$ , while that referring to  $\phi=0.95$  void and interconnect distributions exhibit a shift toward the right of the diameter axis. The interconnect parameter,  $\langle d \rangle / \langle D \rangle$ , remains constant with the variation of  $\phi$ . The thinning of the film of continuous phase

**Table 2.** Morphological Characteristics of Gelatin, Hyaluronic Acid, Chondroitin Sulfate-Methacrylate (G-HA-CS)MA Solid Foams<sup>a</sup>

sample	$C_p$ (% w/v)	$\langle D \rangle^b$ ( $\mu\text{m}$ )	$\sigma_D / \langle D \rangle^c$	$\langle d \rangle^d$ ( $\mu\text{m}$ )	$\sigma_d / \langle d \rangle^e$	$\langle d \rangle / \langle D \rangle^f$
$\phi=0.85$	20	10.8	0.33	5.1	0.35	0.47
$\phi=0.90$	20	12.5	0.36	5.8	0.39	0.46
$\phi=0.92$	25	18.3	0.41	8.2	0.41	0.45
$\phi=0.95$	25	21.6	0.44	10.0	0.46	0.46
$\phi=0.90_{D,0.3}$	20	23.6	0.37	13.5	0.33	0.57
$\phi=0.90_{D,0.6}$	20	28.0	0.43	17.5	0.44	0.61
$\phi=0.90_{D,0.3,S}$	20	32.3	0.43	19.2	0.43	0.59

<sup>a</sup> Obtained by varying the volume percentage of the dispersed phase and the total polymer concentration ( $C_p$ ) in the aqueous phase. <sup>b</sup> Average void diameter. <sup>c</sup> Normalized void diameter polydispersities. <sup>d</sup> Average interconnect diameter. <sup>e</sup> Normalized interconnect diameter polydispersities.

<sup>f</sup> Degree of interconnection.

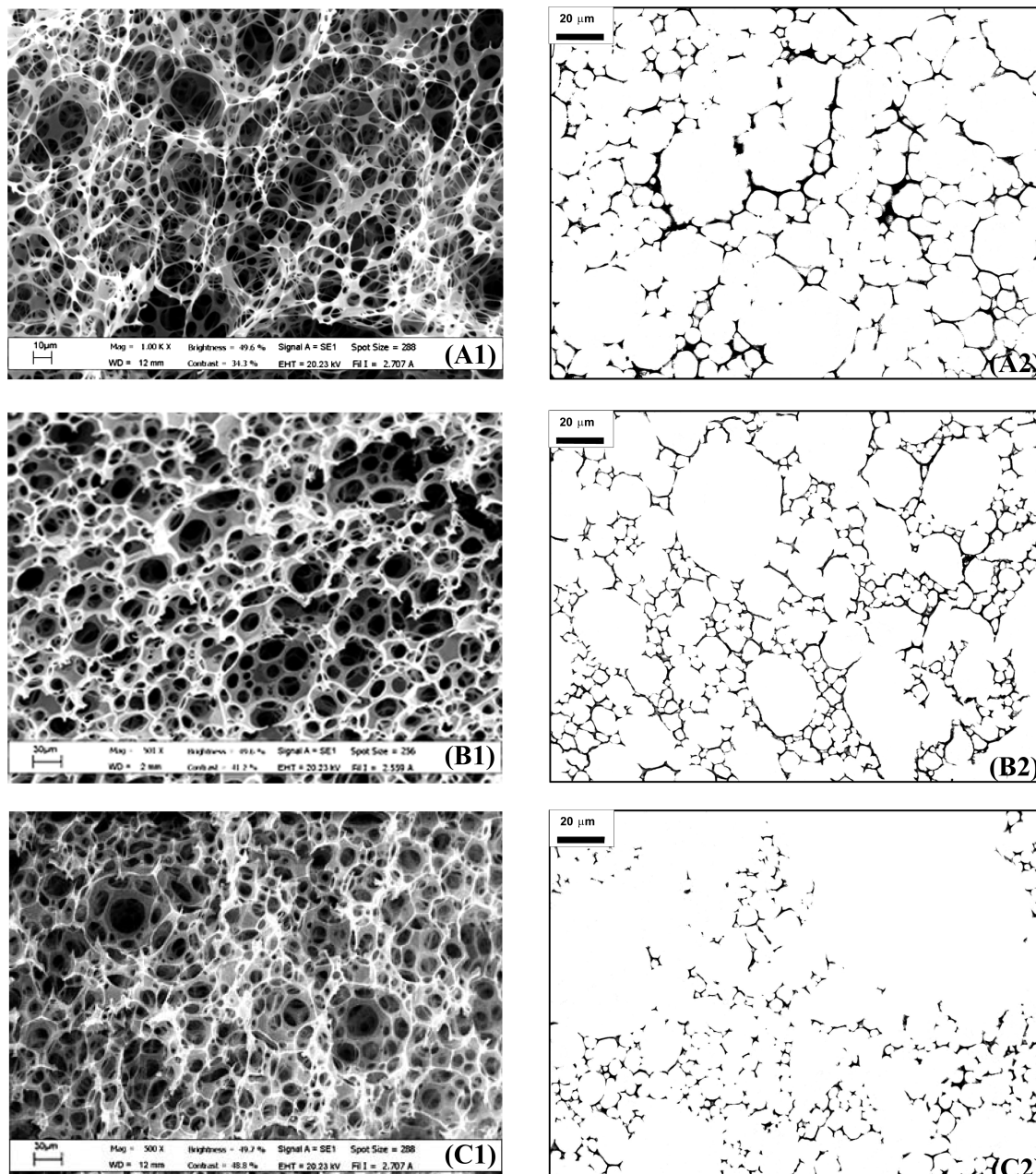


**Figure 3.** Effect of the presence of additives in HIPE formulation: DMSO, 0.3% (A) and 0.6% v/v (B), 0.3% DMSO, NaCl 0.01 M (C) on (G-HA-CS)MA solid foams as evidenced by scanning electron (1) and light microscopy (2) (magnification 200 $\times$ , scale bar 20  $\mu$ m).  $\phi = 0.9$ ;  $C_p = 20\%$  w/v;  $C_s = 7\%$  w/v.

surrounding the droplets of the dispersed phase caused by the increase of  $\phi$  should produce on polymerization larger and larger interconnecting holes with respect to void size (i.e., larger  $\langle d \rangle / \langle D \rangle$ ). The constancy of  $\langle d \rangle / \langle D \rangle$  implies an increase of the interfacial tension ( $\sigma$ ) accompanying the increase of  $\phi$ . In the case  $\phi=0.95$ , the increase of  $\sigma$  seems to be particular relevant as witnessed by the shift of the maxima of the void distribution toward the large diameter side and the constancy of  $\langle d \rangle / \langle D \rangle$  with respect to solid foams with  $\phi < 0.95$ . It is likely that at such a high value of  $\phi$  the amount of the surfactant is not enough to saturate the water/oil interface and the thinning of the film of continuous phase is counterbalanced by the increase of  $\sigma$ , which tends to minimize the interfacial W/O area.

Because the void and interconnect diameters of the solid foams presented in Figure 1 are polydispersed, only those voids and interconnects above a threshold size will be adequate to host cells or cell clusters and allow cell diffusion within the

scaffold volume. As a consequence, it is important to evaluate what % of the scaffold volume is due to voids characterized by a diameter above this threshold and, analogously, the % of the interconnects area attributable to interconnects with a diameter above a certain threshold. Roughly speaking, scaffolds designed for tissue engineering applications should have a significant proportion of voids and interconnects characterized by a size as much as three times and at least equal to the cell dimensions ( $\sim 20\text{ }\mu\text{m}$ ). In Figure 5, such a comparison for the solid foams characterized by increasing  $\phi$  is presented, that is, the cumulative void volume and cumulative interconnect area are plotted against void and interconnect diameters and as a function of  $\phi$ . Only  $\phi=0.92$  and  $\phi=0.95$  have a significant proportion of the scaffold volume attributable to voids characterized by a diameter  $> 40\text{ }\mu\text{m}$  (27 and 30%, respectively) and an interconnect area attributable to interconnects with a diameter  $> 20\text{ }\mu\text{m}$  (10 and 20%, respectively).

From the analysis presented above, it turned out the necessity of improving the scaffolds void and interconnect dimensions.

Previously,<sup>13</sup> we have shown that a considerable increase of void and to a lesser extent in interconnect dimensions can be achieved by causing a partial controlled destabilization in the precursor HIPE. Because emulsions are inherently thermodynamically unstable systems, inducing their partial destabilization, means accelerating the phenomena that leads ultimately to phase separation. Such phenomena are coalescence and Ostwald ripening.<sup>41,42</sup> Coalescence is the irreversible merging of droplets when the thin film between two droplets breaks. Film rupture can be the result of too small a value of the disjoining pressure.<sup>43</sup> Ostwald ripening in emulsion is the growth of bigger droplets at the expense of smaller ones. The driving force of this process is the Laplace pressure, being larger in smaller droplets than in bigger ones. The kinetic of Ostwald ripening is proportional to the solubility of the dispersed phase in the continuous one. One way to enhance these processes is to decrease the efficacy of the surfactant to inhibit the kinetics of these phenomena. To do this, one first has to take into account the chemical nature of the surfactant. Many nonionic surfactants consist of a polyoxyethylene chain and an hydrocarbonic tail (like Triton X-405) representing, respectively, the hydrophilic and hydrophobic portions of the surfactant. One may think to affect either the tendency of the hydrophobic parts of the surfactant to associate in water (i.e., its critical micelle concentration, cmc) or to alter the water–poly(oxyethylene) interactions (i.e., the solvent quality toward the surfactant) and, as a consequence, the geometry of the hydrophilic head as a whole and the surfactant partitioning between water and oil phases. The implementation of this strategy can be accomplished through the use of additives either organic or inorganic. To better illustrate the effect of polar organic (water soluble) additives on emulsion stabilization, it is useful to remind the structure of HIPE. In O/W high internal phase emulsions, the equilibrium phases are an oil phase and an oil-swollen aqueous micellar solution (or O/W microemulsion).<sup>13</sup> Because the surfactant aggregates formed are microemulsion droplets, the critical concentration of surfactant required for microemulsion formation is referred to as the critical microemulsion concentration (*c*<sub>mc</sub>). After reaching this point, the surfactant chemical potential stays essentially constant, because all the surfactant added is consumed by the micelles. The interfacial tension at the *c*<sub>mc</sub> is the lowest possible under the given experimental conditions. The presence of a polar component in the organic phase decreases the energy requirements of bringing the hydrophobic tails of the surfactant into solution leading to an increase in *c*<sub>mc</sub>. In this way, the equilibrium between the microemulsion phase and the surfactant interfacial layer is unbalanced. As a consequence, some surfactant molecules are driven off the interface to restore the equilibrium. Furthermore, DMSO renders the organic phase a better solvent for the surfactant with the consequence that the equilibrium of partitioning of the surfactant between the water and organic phases is shifted to some extent in favor of the organic phase. In such circumstances, the interfacial layer may not be saturated anymore with surfactant molecules and thus less robust and more prone to break down following a collision between droplets of the dispersed phase. In the extreme case, coalescence phenomena may occur.

In an attempt to destabilize the HIPE in a controlled manner, such an approach was implemented. A very small amount of DMSO was added (0.3% v/v with respect to the organic phase) to the HIPE characterized by a  $\phi = 0.90$ . It is evident from SEM and LM micrographs (Figure 3A1,A2) that even a small

amount of DMSO has a pronounced effect on the solid foam morphology. The resulting void diameter distribution (Figure 4A1) is broader than that  $\phi 0.90$  (Figure 2b1). The LM micrograph of  $\phi 0.90_{D0.3}$  reminds that referring to  $\phi 0.95$  and such similarity is qualitatively confirmed by the comparison between the void diameter distributions: both distributions span over the same diameter range and have the maxima positioned approximately at the same value of *D*. The *d* distribution of  $\phi 0.90_{D0.3}$  is shifted toward higher diameter side than that referring to  $\phi 0.95$  and as a result its  $\langle d \rangle$  is higher. Thus, the addition of small quantity of DMSO in HIPE formulation simulates very high  $\phi$ . At this point it seemed natural to increase the amount of DMSO added (0.6% v/v). In Figure 3B1,B2 the SEM and LM of  $\phi 0.90_{D0.6}$  are shown. From the LM micrograph it is evident that the precursor HIPE underwent, prior to gelation, coalescence to some extent, as evidenced by the presence of partially or completely merged voids, the latter being characterized by an ellipsoidal symmetry.

The void distribution (Figure 4B1) of  $\phi 0.90_{D0.6}$  exhibits a maximum at the same position as that of  $\phi 0.90_{D0.3}$  but a longer tail in the high diameter side that supports the hypothesis of the occurrence of coalescence phenomena. The gain in  $\langle D \rangle$  and  $\langle d \rangle$  (Table 2) is not particularly relevant and both polydispersities  $\sigma_D/\langle D \rangle$  and  $\sigma_d/\langle d \rangle$  increase as a result of enhanced emulsion instability induced by the increase in DMSO content.

Use of larger amount DMSO failed at giving porous materials with a well-defined morphology. This result contrasts with the solid foams obtained previously by using GMA only.<sup>13</sup> In that case, an amount of DMSO as large as 1% v/v could be successfully employed without inducing a too pronounced emulsion destabilization and allowed to obtain materials ( $\phi = 0.9$ ) with a  $\langle D \rangle$  and  $\langle d \rangle$  of 61 and 18  $\mu\text{m}$ , respectively. It may be wondered the reason of the higher sensitivity of the HIPEs of the present work toward DMSO. It is clear that the origin of this difference resides on HIPE composition, in other words, on the presence of a significant amount of polyelectrolytes with high charge density (HA and CS). HA bears a sodium-carboxylate group in each repeating unit, while CS bears a sodium-carboxylate and sodium-sulfate group in each repeating unit.

It is well-known that the HLB (hydrophilic lipophilic balance) of a nonionic surfactant of the poly(ethylene oxide)/hydrocarbon type can be made more lipophilic upon addition of salting out electrolytes, as indicated by the depressed PIT (phase inversion temperature) values. The study of the phase behavior of oil–water–surfactant system at constant temperature, in particular, of the so-called middle phase using low interfacial measurements, indicates that electrolytes such as NaCl, KCl, or CaCl<sub>2</sub> enhance partitioning of the surfactant into the oil phase, thus decreasing its effective HLB. Several workers observed that the effect of added electrolytes, as shown in phase diagrams, was in many respects similar to that of temperature, at least in the neighborhood of the PIT. Small hydrated ions with low lyotropic number are more effective in salting out and consequently decreasing the HLB of nonionic surfactants than large hydrated ions (with large lyotropic number). Shinoda and Takeda<sup>44</sup> showed that the presence of 6 wt % of NaCl in water corresponds to a decrease of the PIT by about 14 °C or of the HLB value by about 1.2. Electrolytes, such as KSCN, affect the structure of water by promoting its depolymerization, thus increasing the hydration of polyoxyethylene chains and raising its cloud point as well as the HLB (salting in). Similarly, the nitrates of multivalent cations which form stable complex with

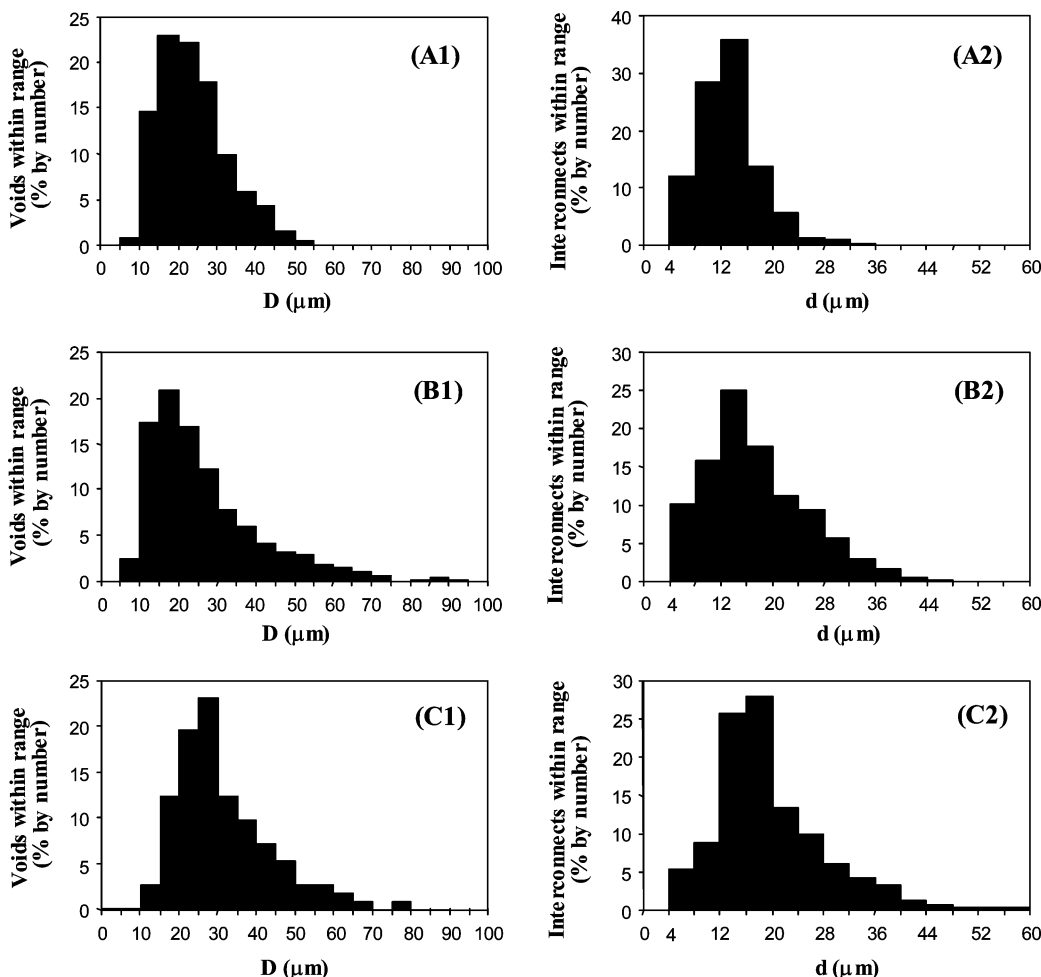


**Figure 4.** Effect of the presence of additives in HIPE formulation (DMSO and NaCl) on the number-distribution of voids (1) and interconnects (2) size of (G-HA-CS)MA solid foams. (A) 0.3% v/v, (B) 0.6% v/v of DMSO, (C) 0.3% v/v of DMSO and 0.01 M NaCl. Percentages refer to the dispersed phase.  $\phi = 0.90$ . Surfactant concentration  $C_s = 7\%$  w/v. Polymer concentration  $C_p = 20\%$  w/v. The area of a histogram bar is proportional to the number-fraction of either voids or interconnects within a size range.

the oxygen atom of the polyoxyethylene raise the cloud point and the HLB. Furthermore, the effect of anions is more marked than that of cations, as shown by the cloud point measurements.<sup>45</sup> On the contrary, anions that promote the water structure or bind water molecules extensively, such as  $\text{OH}^-$ ,  $\text{F}^{-1}$ ,  $\text{Cl}^{-1}$ ,  $\text{SO}_4^{=2}$ , and  $\text{PO}_4^{=3}$ , suppress the cloud point.<sup>46</sup> The order of the anions that cause the change of HLB agrees generally with the lyotropic series.

It is then plausible that the HIPE containing NaHAMA and NaCSMA (all the other physical parameters kept fixed) will be less stable than that containing GMA only. Therefore, they are more sensitive to destabilizing additives. As a confirmation of the hypothesis outlined above and in an attempt to improve further the morphological characteristics of our scaffolds, the effect of inorganic additives, namely, NaCl, besides DMSO, was explored. As stated above, NaCl exerts a salting out effect on nonionic surfactants like Triton X405 and, thus, causes an increase of  $\sigma$ . NaCl was dissolved in the aqueous phase of the emulsion at a concentration of 0.01 M. As expected, very large voids (Figure 3C) appeared in the scaffold porous structure and the void distribution (Figure 4C1) presented a maximum shifted slightly toward the high diameter side with respect to that referring to  $\phi 0.90_{\text{D},0.6}$ . Comparing the behavior of the cumulative void volumes (Figure 5b1) of the scaffolds obtained with the use of additives, it is evident that  $\phi 0.90_{\text{D},0.6}$  has the largest percentage of the scaffold volume attributable to voids with  $D$

$\geq 40 \text{ m}\mu$  (77%) or  $\geq 60 \text{ m}\mu$  (44%), while for  $\phi 0.90_{\text{D},0.3,\text{S}}$ , these percentages are 73 and 32%, respectively. As far as interconnects are concerned, Figure 5b2 shows a reversed trend,  $\phi 0.90_{\text{D},0.3,\text{S}}$  has 87 or 43% of the interconnect area attributable to interconnects with a  $d \geq 20 \text{ }\mu\text{m}$  or  $\geq 30 \text{ }\mu\text{m}$ , respectively, while for  $\phi 0.90_{\text{D},0.6}$ , such percentages are 79 or 31%. Overall, both  $\phi 0.90_{\text{D},0.6}$  and  $\phi 0.90_{\text{D},0.3,\text{S}}$  scaffolds present, among the scaffolds synthesized, the best morphological characteristics. In cell culture tests described in the following section  $\phi 0.90_{\text{D},0.6}$  will be used.

**In Vitro Biodegradation.**<sup>47</sup> A key feature a scaffold for tissue engineering applications must possess is the ability to degrade in a physiological environment to allow the proliferating cells to replace gradually the scaffold itself.

For this reason, the degradation in vitro of both GMA and (G-HA-CS)MA scaffolds by proteinases, that is, under cell-free conditions, was studied. The kinetics of scaffold degradation was monitored with a spectrophotometric assay that measures the appearance of solubilized hydrolysis products during the reaction. It must be stressed that the concentration of the proteinase used was much higher than that normally found in the human body. As it is evident from Figure 6 the evolution of scaffold hydrolysis is steeper in the case of GMA scaffold than in (G-HA-CS)MA. The former was completely degraded in about 100 h, while (G-HA-CS)MA required an exposure time

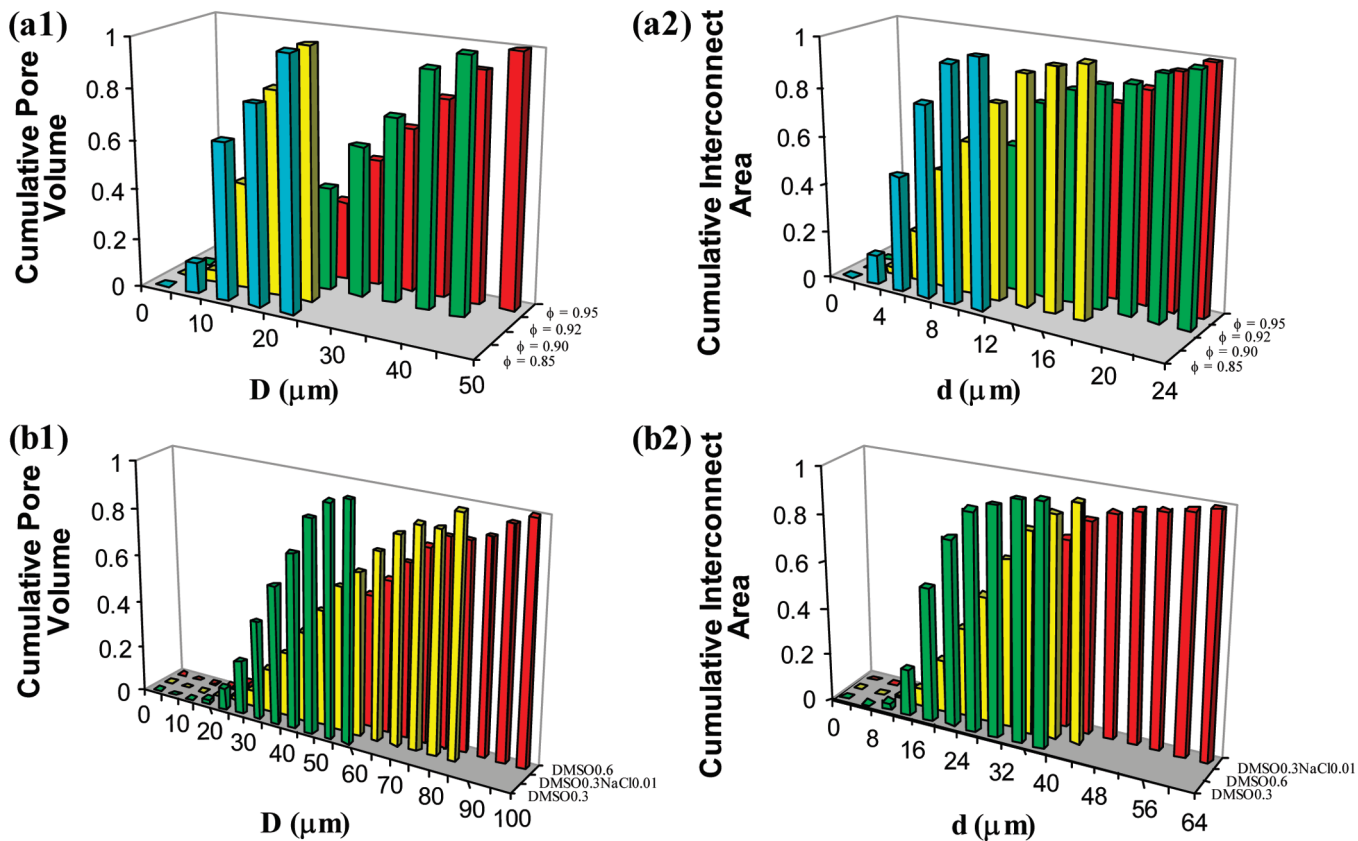


**Figure 5.** Cumulative void volume (1) and cumulative interconnect area (2) of (a) solid foams characterized by increasing volume fraction of the dispersed phase  $\phi$  or (b) obtained by keeping  $\phi$  constant at 0.9 and by using additives (DMSO and NaCl, 0.01 M).

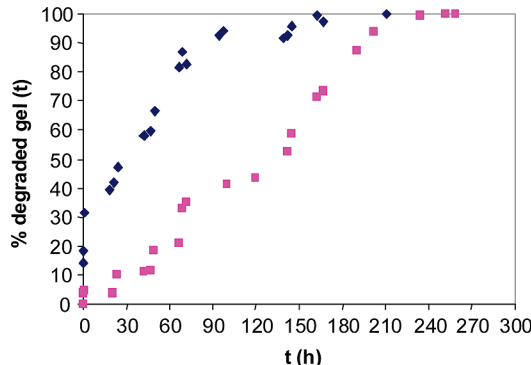


**Figure 6.** Typical degradation kinetics of GMA (◆) and (G-HA-CS)MA (red square) scaffolds. The solubilization was catalyzed by thermolysin at 37 °C.

to proteinase as long as double to be completely dissolved. There are two possible reasons for such a behavior: (1) The higher cross-linking density of the (G-HA-CS)MA scaffold. HAMA and CSMA have a relatively higher density of methacrylate functionalities than GMA. This gives rise on polymerization to a network more heavily cross-linked than GMA scaffold and, thus, more resistant to enzymatic degradation. (2) The content of gelatin in (G-HA-CS)MA scaffolds is 20% w/v lower than in GMA one. Thus, the sites of thermolysine attack may be partially screened by HA and CS chains. Furthermore, the ionic strength associated to the presence of charged groups belonging to HA and CS may lower the activity of thermolysine.

**Cell Studies.** The two different types of scaffolds were tested in hepatocyte studies, using the human hepatic cell line C3A. Advantages of using a cell line in contrast to primary cells include stability, ease of proliferation, and possibility of long-term maintenance. In particular, C3A cells, although clonal

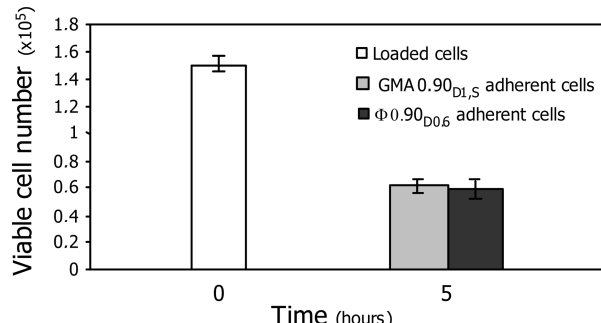


**Figure 7.** Initial C3A cell adhesion. CA3 cells were seeded at 0.15 × 10<sup>6</sup> cells per scaffold (either GMA 0.90<sub>D1,S</sub> or φ 0.90<sub>D0,6</sub>) in 24-well culture plates. Five hours after seeding, the medium with unattached cells was removed and the viability of adherent cells was evaluated by a MTS assay. A standard curve was assessed to convert O.D. values to number of viable cells. The results are the mean of three samples from four different experiments ± SD.

derivatives of the widely used human hepatoma cell line HepG2, display an improved differentiated hepatocyte phenotype, thus representing a good human model for in vitro studies. C3A cells have already been used in three-dimensional cultures, as well as in clinical trials using bioartificial liver devices.<sup>48–50</sup>

Cell adhesion and viability within the scaffolds were analyzed during the culture period using MTS, a compound that can only be metabolized by healthy cells. Data were converted to viable cell number using a calibration curve, which allowed us to calculate, at each time point, the number of viable cells in the different cell-seeded biomaterials. The number of adherent viable cells was first evaluated after 5 h of incubation. As indicated in Figure 7, about 40% of C3A cells attached to GMA 0.90<sub>D1,S</sub> scaffolds as well as to φ 0.90<sub>D0,6</sub>, thus showing that initial cell

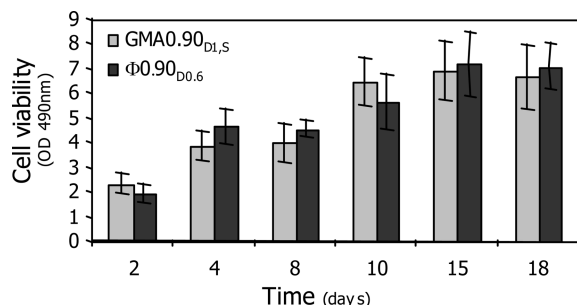


**Figure 8.** MTS assay. C3A cell viability was measured by a MTS assay at 2, 4, 8, 10, 15, and 18 days and reported as O.D. values. The results are the mean of four samples from three different experiments  $\pm$  SD.

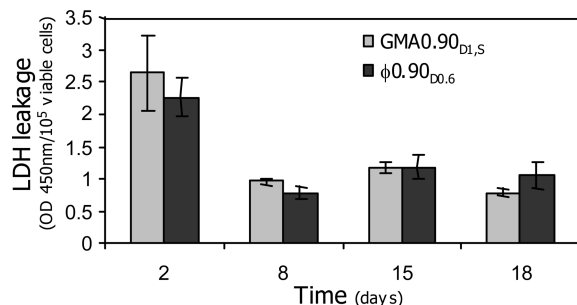


**Figure 9.** Assessment of cell damage by LDH leakage. Enzyme level was determined at 2, 8, 15, and 18 days and normalized to the number of viable cells per well. Data represent the mean  $\pm$  SD of four samples from three different experiments.

affinities were similar with the two different matrices. Thereafter, cells maintained good viability with no significant differences, in either GMA0.90<sub>D<sub>1,S</sub></sub> or ϕ0.90<sub>D<sub>0,6</sub></sub> scaffolds. After a first growth phase, the MTS assay showed a constant number of cells during the second week of culture (8–18 days), suggesting that cell proliferation was limited or balanced by cell death (Figure 8).

To better discriminate between cell proliferation and cell damage within the different scaffolds, LDH leakage was monitored in the cell supernatant of the long-term cultures and normalized to the number of viable cells. As Figure 9 shows, after an initial peak, cell damage appeared acceptably low and constant throughout the culture period, with no significant differences between the two scaffolds. These results demonstrate as well the good biocompatibility of our biomaterials.

The ratio of live to dead cells was also visualized on the confocal microscope using a two-color fluorescence assay, as reported in Materials and Methods. Fluorescence micrographs clearly show that most cells in the aggregates were stained fluorescent green (viable), while the number of red dead cells was minor and quite constant during the culture period (Figure 10).

The ultrastructural analysis, performed by SEM, showed that C3A cells adhered on both of the tested biomaterials, with a homogeneous colonization of the scaffolds (Figure 11). A few days postseeding, C3A cells appeared as individuals or as small multicellular aggregates (Figure 11a,d). Starting from 8 days postseeding, larger and more compact spheroid-like cell aggregates were found in both scaffolds (Figure 11b,e), consisting of cuboidal-shaped cells with abundant and regular microvilli (Figure 11c,f). Cells growing in spheroid-like aggregates are a common trait of cell line cultures and is indicative of a greater number of interactions between adjacent cells, rather than with

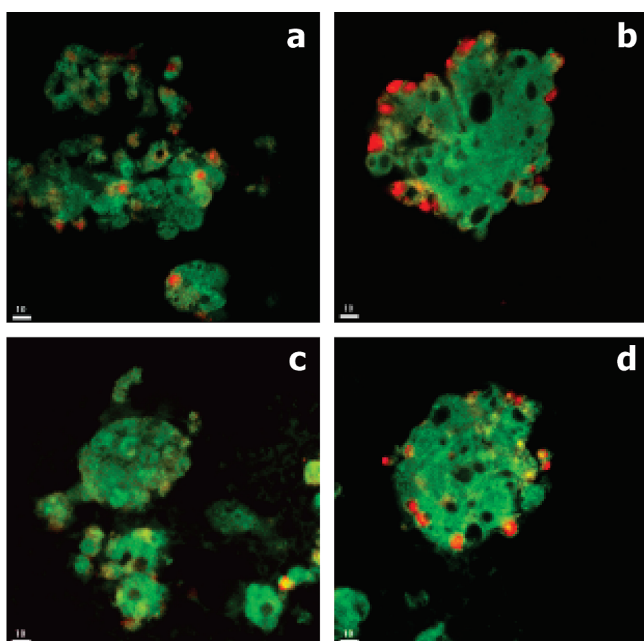


**Figure 10.** Live/dead cell test. Confocal micrographs of SYTO-10/DEAD-Red double-stained C3A spheroids within GMA0.90<sub>D<sub>1,S</sub></sub> and ϕ0.90<sub>D<sub>0,6</sub></sub> scaffolds 4 and 10 days postseeding. Most cells in aggregates are stained only fluorescent green (viable).

the scaffolds themselves, which may support their polarity and their ability to perform normal metabolic activity (e.g., albumin secretion).

In addition, cells always showed regular and numerous microvilli on their surface, as expected for normal, healthy cells (Figure 11c,f).<sup>50,51</sup> C3A functionality and, thus, the general efficiency of the system were estimated by analyzing albumin secretion, a typical product of hepatocytes, generally recognized as an indicator of liver-specific functions.<sup>52</sup> Two different approaches were utilized to estimate albumin production in long-term cultures. As we found that initial cell adhesion as well as cell growth during the total culture period were similar with both biomaterials, we prepared cell-seeded constructs in quadruplicate and assessed a time course of albumin secretion by quantifying the protein produced by the same cells during the culture. In parallel experiments, the albumin secretion was measured in different wells but at each time point values were normalized to the number of viable cells present in that well. As expected, the two different approaches produced very similar results (Figure 12a,b).

Specific albumin secretion started at two days and increased with the time of culture reaching maximum values between days 10 and 15 postseeding. At these time points, albumin secretion was significantly higher in ϕ0.90<sub>D<sub>0,6</sub></sub> as compared to GMA0.90<sub>D<sub>1,S</sub></sub>. Nevertheless, in both materials, the levels of albumin production were considerably elevated, also in comparison with literature data,<sup>53,50</sup> thus proving the efficiency of our systems in restoring liver functions. To further confirm the validity of our tridimensional scaffolds, similar experiments were performed in monolayer, either on polystyrene or gelatine-coated polystyrene plates. C3A cells grown in monolayer produced much lower levels of albumin, validating the suitability of our three-dimensional constructs (Figure 12a,b).

## Conclusions

In this work we successfully prepared, for the first time, scaffolds that include gelatin and GAGs in combination with

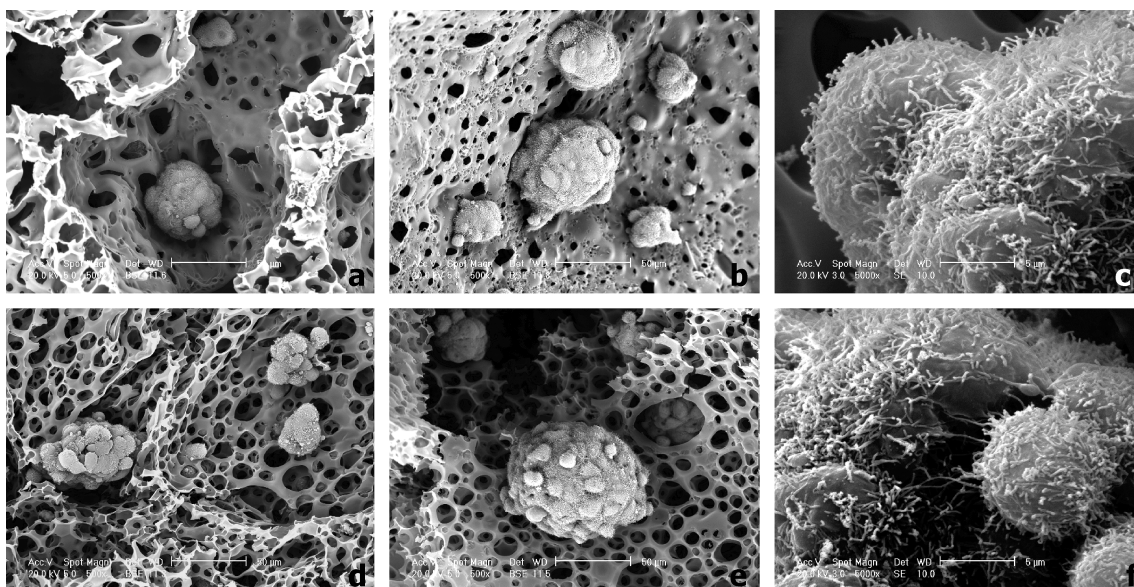


**Figure 11.** Scanning electron micrographs of C3A cells were cultured for either 4 (a, c, d, f) or 10 (b, e) days on GMA $0.90_{D1,S}$  (a,b,c) or  $\phi0.90_{D0,6}$  (d,e,f) scaffolds. Well-organized cell aggregates can be observed within both scaffolds. At day 10, postseeding bigger and more compacted cell-spheroids were seen. Higher magnifications show details of cell surfaces, displaying abundant and regular microvilli (c, f).

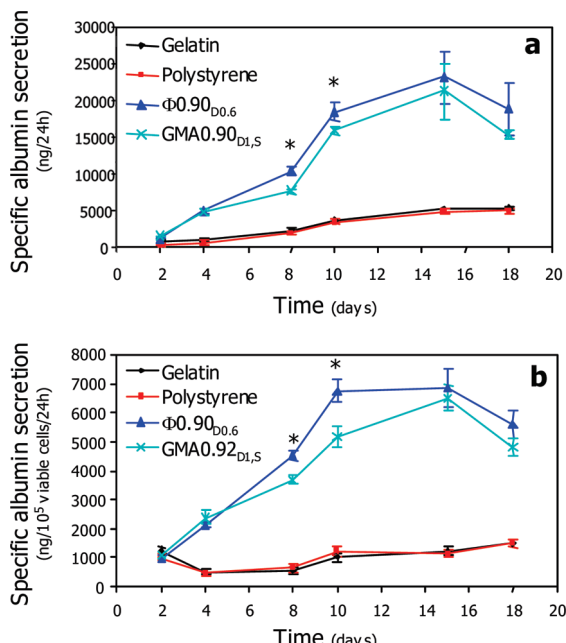


**Figure 12.** Specific albumin secretion. Cells were grown for 18 days either in GMA $0.90_{add}$  and  $\phi0.90_{D0,6}$  scaffolds or in monolayer using polystyrene or gelatine matrices. (a) Time course of albumin production by single-well C3A cells. (b) Specific albumin secretion from C3A-seeded scaffolds cultured for 2, 4, 6, 8, 10, 15, or 18 days. At each time point, the secretion rate was normalized to the number of viable cells, based on the MTS assay. All results are the mean  $\pm$  SD of three samples from three different experiments. \* $P < 0.05$ .

emulsion templating as the synthetic technique. The scaffold morphology (dimension of voids and interconnects) can be tailored, to the first instance, by simply varying the volume fraction of the dispersed phase and, second, by affecting the emulsion stability through the use of additives (either organic or inorganic). These additives influence both the extent of aggregation of the surfactants dissolved in the aqueous phase and the geometry of the hydrophilic head of the surfactants adsorbed at the oil/water interface as well as its level of partitioning between the aqueous and oil phase. In this way,

supports with a significant proportion of voids and interconnects suitable for cell colonization could be synthesized.

One of the aims of this work was to assess if the inclusion of GAGs into the scaffold formulation resulted in an improvement of the biocompatibility with respect to scaffolds obtained by using GMA only. To this end, hepatocytes were cultured on both kinds of scaffolds (GMA $0.90_{D1,S}$  and  $\phi0.90_{D0,3,S}$ ), and assessments of cell viability and function were performed. Although the scaffold containing GAGs did not exhibit superior performances as far as cell colonization and ratio of alive/dead cells over GMA scaffold, the secretion of albumin was significantly higher in the former scaffold. This result is encouraging since albumin is one of the most important functional marker proteins in the liver and an increase in its expression implies a closer resemblance to the *in vivo* hepatocyte physiology. Another advantage of (G-HA-CS)MA over GMA scaffolds resides in the higher resistance to enzymatic degradation, which would ensure a longer permanence of the scaffold *in vivo*.

Nevertheless, the presence of poly(methylmethacrylate) chains bridging gelatin, HA, and CS presumably partially offsets the beneficial effects of GAGs. Furthermore, it is likely that part of the methacrylic moieties (especially in HAMA, the biopolymer among those used in this work with the highest degree of functionalization (30%)) are left unreacted in the final scaffold. Such a methacrylic group may be subject to attack (Michael addition) from nucleophilic groups such as the primary amines of the lysine residues of cell membrane proteins increasing the cytotoxicity of the scaffolds. These hypotheses would be in line with the results found previously,<sup>23</sup> that is, gelatin scaffolds cross-linked enzymatically with transglutaminase exhibited pronouncedly better biocompatibility over GMA-based scaffolds. These hypotheses are being currently evaluated and will be the object of a shortcoming publication.

**Acknowledgment.** The authors thank the University of Rome “La Sapienza” (Ateneo funds) and Consorzio Interuniversitario (CIB) for funding this research and Dr. Daniela Ferro for invaluable help with the scanning electron microscope.

**Supporting Information Available.** Kinetic of hyaluronic acid degradation by HYASE, viscosity, and GPC measurement results on solutions of hyaluronic acid and its degradation product, NMR spectra of methacrylated hyaluronic acid and chondroitin sulfate, and EDS spectrum and EDS map of a scaffold. This information is available free of charge via the Internet at <http://pubs.acs.org>.

## References and Notes

- (1) Bell, E. *Tissue Eng.* **1995**, *1*, 163–179.
- (2) Liu, W.; Merrett, K.; Griffith, M.; Fagerholm, P.; Dravida, S.; Heyne, B.; Scaiano, J. C.; Watsky, M. A.; Shinozaki, N.; Lagali, N.; Munger, R.; Li, F. *Biomaterials* **2008**, *29*, 1147–1158.
- (3) Barnes, C. P.; Pemble, C. W.; Brand, D. D.; Simpson, D. G.; Bowlin, G. L. *Tissue Eng.* **2007**, *13*, 1593–1605.
- (4) Riesle, J.; Hollander, A. P.; Langer, R.; Freed, L. E.; Vunjak-Novakovic, G. *J. Cell. Biochem.* **1998**, *71*, 313–327.
- (5) Barnes, C. P.; Pemble, C. W.; Brand, D. D.; Simpson, D. G.; Bowlin, G. L. *Tissue Eng.* **2007**, *13*, 1593–1605.
- (6) Guidoin, R.; Marceau, D.; Reo, T. J.; King, M.; Mahi, Y.; Roy, P. E. *Biomaterials* **1987**, *8*, 433–441.
- (7) Tabata, Y.; Hijikata, S.; Ikada, Y. *J. Controlled Release* **1994**, *31*, 189–199.
- (8) Choi, Y. S.; Hong, S. R.; Lee, Y. M.; Song, K. W.; Park, M. H.; Nam, Y. S. *Biomaterials* **1999**, *20*, 409–417.
- (9) Li, X.; Jin, L.; Balian, G.; Laurencin, C. T.; Anderson, D. G. *Biomaterials* **2006**, *27*, 2426–2433.
- (10) Lee, J.; Tae, G.; Kim, Y. H.; Park, I. S.; Kim, S.-H.; Kim, S. H. *Biomaterials* **2002**, *23*, 1872–1879.
- (11) Rohanizadeh, R.; Swain, M. V.; Mason, R. S. *J. Mater. Sci.* **2008**, *19*, 1173–1182.
- (12) Barbetta, A.; Dentini, M.; De Vecchis, M. S.; Filippini, P.; Formisano, G.; Caiazza, S. *Adv. Funct. Mater.* **2005**, *15*, 118–124.
- (13) Barbetta, A.; Dentini, M.; Zannoni, E. M.; De Stefano, M. E. *Langmuir* **2005**, *21*, 12333–12341.
- (14) Palocci, C.; Barbetta, A.; La Grotta, A.; Dentini, M. *Langmuir* **2007**, *23*, 8243–8251.
- (15) Barbetta, A.; Massimi, M.; Conti Devirgiliis, L.; Dentini, M. *Biomacromolecules* **2006**, *7*, 3059–3068.
- (16) Jackson, R. I.; Busch, S. J.; Cardin, A. D. *Physiol. Rev.* **1991**, *71*, 481–539.
- (17) Roskam, T.; Moshage, H.; Vos, R. D.; Guido, D.; Yap, P.; Desmet, V. *Hepatology* **1995**, *21*, 950–958.
- (18) Park, Y. D.; Tirrelli, N.; Hubbel, J. A. *Biomaterials* **2003**, *24*, 893–900.
- (19) Choi, Y. S.; Hong, S. R.; Lee, Y. M.; Song, K. W.; Park, M. H.; Nam, Y. S. *J. Biomed. Mater. Res.* **1999**, *14*, 631–639.
- (20) Benedetti, L.; Cortivo, R.; Berti, A.; Pea, F. *Biomaterials* **1993**, *14*, 1154–1158.
- (21) Larsen, N. E.; Pollak, C. T.; Reiner, K.; Leshchiner, E.; Balsas, E. A. *J. Biomed. Mater. Res.* **1993**, *27*, 1129–1132.
- (22) Burdick, J. A.; Chung, C.; Jia, X.; Randolph, M. A.; Langer, R. *Biomacromolecules* **2005**, *6*, 386–391.
- (23) Sherman, L.; Leeman, J.; Herrlich, P.; Ponte, H. *Curr. Opin. Cell Biol.* **1994**, *6*, 726–733.
- (24) Jia, X.; Yeo, Y.; Clifton, R. J.; Jiao, T.; Kohane, D. S.; Kobler, J. B.; Zeitels, S. M.; Langer, R. *Biomacromolecules* **2006**, *7*, 3336–3344.
- (25) Vercruyse, K. P.; Lauwers, A. R.; Demeester, J. M. *J. Chromatogr., B: Biomed. Sci. Appl.* **1994**, *656*, 179–190.
- (26) Busby, W.; Cameron, N. R.; Jahoda, C. A. *Biomacromolecules* **2001**, *2*, 154–164.
- (27) Christenson, E. M.; Soofi, W.; Holm, J. L.; Cameron, N. R.; Mikos, A. G. *Biomacromolecules* **2007**, *8*, 3806–3814.
- (28) Bokhari, M.; Carnachan, R. J.; Cameron, N. R.; Przyborski, J. *J. Anat.* **2007**, *211*, 567–576.
- (29) Bokhari, M.; Carnachan, R. J.; Cameron, N. R.; Przyborski, J. *Biochem. Biophys. Res. Commun.* **2007**, *354*, 1095–1100.
- (30) Hayman, M. W.; Smith, K. H.; Cameron, N. R.; Przyborski, J. *J. Biophys. Biochem. Methods* **2005**, *62*, 231–240.
- (31) Hayman, M. W.; Smith, K. H.; Cameron, N. R.; Przyborski, J. *Biochem. Biophys. Res. Commun.* **2004**, *314*, 483–488.
- (32) Akay, G.; Birch, M. A.; Bokhari, M. *Biomaterials* **2004**, *25*, 3991–4000.
- (33) Mendichi, R.; Söltes, L.; Schieroni, A. G. *Biomacromolecules* **2003**, *4*, 1805–1810.
- (34) Roden, L.; Campbell, P.; Fraser, J. R. E.; Laurent, T. C.; Pertoft, H.; Thompson, J. N. In *The Biology of Hyaluronan*; Ciba Foundation Symposium 143, Evered, D., Whelan, J., Eds.; John Wiley: Chichester, 1989.
- (35) Wang, L.-F.; Shen, S.-S.; Lu, S.-C. *Carbohydr. Polym.* **2003**, *52*, 389–396.
- (36) Princen, H. M.; Kiss, A. D. *J. Colloid Interface Sci.* **1989**, *128*, 176.
- (37) Otsubo, Y.; Prud'homme, R. K. *Rheol. Acta* **1994**, *33*, 29.
- (38) Kawaguchi, M.; Tsujino, T.; Kato, T. *Langmuir* **2000**, *16*, 5568.
- (39) Das, A. K.; Mukesh, D.; Swayambunathan, V.; Kotkar, D. D.; Ghosh, P. K. *Langmuir* **1992**, *8*, 2427.
- (40) Hayakawa, K.; Kawaguchi, M.; Kato, T. *Langmuir* **1997**, *13*, 6069.
- (41) Leal-Calderon, F.; Schmitt, V.; Bibette, J. *Emulsion Science. Basic Principles*, 2nd ed.; Springer: New York, 2007.
- (42) Taylor, P. *Adv. Colloid Interface Sci.* **1998**, *75*, 107–163.
- (43) (a) Derjaguin, B. V.; Obukov, E. V. *Acta Physicochim. URSS* **1936**, *5*, 1. (b) Derjaguin, B. V. *Theory of Stability of Colloids and Thin Liquids Films*; Plenum/Consultants Bureau: New York, 1989.
- (44) Shinoda, K.; Takeda, H. *J. Colloid Interface Sci.* **1970**, *32*, 642.
- (45) (a) Marzsall, L. *Tenside, Surfactants, Deterg.* **1981**, *18*, 25-. (b) Schick, M. J. *J. Colloid Sci.* **1962**, *17*, 801.
- (46) (a) Schott, H.; Royce, A. E. *J. Pharm. Sci.* **1984**, *73*, 793–799. (b) Schott, H.; Royce, A. E.; Han, S. K. *J. Colloids Interface Sci.* **1984**, *98*, 196–201.
- (47) (a) Fadda, G. C.; Lairez, D.; Arrio, B.; Carton, J.-P.; Larreta-Garde, V. *Biophys. J.* **2003**, *85*, 2808–2817. (b) Berry, H.; Pelta, J.; Lairez, D.; Larreta-Garde, V. *Biochim. Biophys. Acta* **2000**, *1524*, 110–117.
- (48) Filippi, C.; Keatch, S. A.; Rougar, D.; Nelson, L. J.; Hayes, P. C.; Plevris, J. N. *J. Hepatol.* **2004**, *41*, 599–605.
- (49) Park, J. K.; Lee, D. H. *J. Biosci. Bioeng.* **2005**, *99*, 311–319.
- (50) Elkayam, T.; Amitay-Shaprut, S.; Dvir-Ginzberg, M.; Harel, T.; Cohen, S. *Tissue Eng.* **2006**, *12* (5), 1357–1368.
- (51) Dvir-Ginzberg, M.; Elkayam, T.; Aflalo, E. D.; Agraria, R.; Choen, S. *Tissue Eng.* **2004**, *10*, 1806–1815.
- (52) Kane, B. J.; Zinner, M. J.; Yarmush, M. L.; Toner, M. *Anal. Chem.* **2006**, *78*, 4291–4298.
- (53) Krasteva, N.; Harms, U.; Seifert, B.; Albrecht, W.; Hopp, M.; Altankov, G.; Groth, T. *Biomaterials* **2002**, *24*, 2467–2478.

BM800599D